QUANTUM SIMULATION

Microscopic evolution of doped Mott insulators from polaronic metal to Fermi liquid

Joannis Koepsell[1,2]*, Dominik Bourgund[1,2], Pimonpan Sompet[1,2], Sarah Hirthe[1,2], Annabelle Bohrdt[2,3]†‡, Yao Wang[4,5], Fabian Grusdt[2,6], Eugene Demler[4]§, Guillaume Salomon[1,2,7,8], Christian Gross[1,2,9], Immanuel Bloch[1,2,6]

The competition between antiferromagnetism and hole motion in two-dimensional Mott insulators lies at the heart of a doping-dependent transition from an anomalous metal to a conventional Fermi liquid. We observe such a crossover in Fermi-Hubbard systems on a cold-atom quantum simulator and reveal the transformation of multipoint correlations between spins and holes upon increasing doping at temperatures around the superexchange energy. Conventional observables, such as spin susceptibility, are furthermore computed from the microscopic snapshots of the system. Starting from a magnetic polaron regime, we find the system evolves into a Fermi liquid featuring incommensurate magnetic fluctuations and fundamentally altered correlations. The crossover is completed for hole dopings around 30%. Our work benchmarks theoretical approaches and discusses possible connections to lower-temperature phenomena.

Interacting electrons in conventional metals are successfully described by Landau's Fermi liquid (FL) theory, which captures the universal behavior of macroscopic properties. The violation of the concepts underlying FL theory is a hallmark of strongly correlated quantum materials, leading to phenomena such as pseudogap or strange metal regimes (*1*). In this context, doped antiferromagnetic Mott insulators are particularly interesting, because they exhibit non-FL behavior for weak doping but turn into normal FLs for high doping (*1*–*3*). Furthermore, these systems often host unconventional superconductivity. The highest transition temperatures in hole-doped cuprates occur in the same range of doping as the strange metal phase, which indicates a strong relation between the two phenomena.

Recent studies on cuprates suggest that a transition from unconventional metal to FL occurs at a hole doping of $\delta^* \approx 20\%$ (*4*, *5*); the exact value of δ^* is expected to be material dependent. Spectroscopy and transport measurements hint at charge carriers being "hole-like" below and "particle (electron)–like" above this hole concentration (*5*–*7*). Nonetheless, the interpretation and universality of such findings is unclear, owing to the microscopic complexity of real materials.

In Mott insulators slightly below half filling, the competition between hole motion and antiferromagnetism leads to heavily dressed dopants (*8*, *9*), referred to as magnetic polarons (*10*–*16*). The interplay between magnetism and hole hopping remains relevant up to intermediate dopings (*17*) and is believed to ultimately trigger pseudogap and superconducting phases at colder temperatures (*1*, *3*). A generally accepted description of these phenomena in terms of interacting magnetic polarons, spin-liquid states, or other microscopic models remains elusive. For large dopings, antiferromagnetic correlations become strongly suppressed, particle motion is restored in the dilute system, and FL-type quasiparticles form. At which hole concentration magnetic polarons dissolve, whether exotic regimes result from interactions of polarons, and how local correlations in the polaronic and the FL regime are connected constitute essential questions of the high-temperature superconductivity puzzle.

A paradigmatic description of strongly correlated quantum materials is the two-dimensional (2D) Fermi-Hubbard model. Despite recent progress in its numerical analysis (*18*, *19*), a thorough understanding of this model is still lacking, making it a primary target for quantum simulation. The model consists of spin-1/2 fermions on a lattice with nearest-neighbor (NN) tunneling amplitude t and on-site repulsion U, which leads to antiferromagnetic spin couplings J. Cold atom–based quantum simulators provide fully tunable implementations of such systems with single-site resolved readout and continuous doping control (*20*). Recent studies of systems in and out of equilibrium have characterized transport coefficients (*21*, *22*) and two-point correlations (*23*–*26*) in doped Mott insulators. The advent of full spin and density resolution (*27*, *28*) enabled imaging of the dressing cloud of magnetic polarons (*29*) and the exploration of spin-charge separation in one dimension (*30*–*32*) through the measurement of spin-charge correlators.

In this study, we examined the hole-doping dependence of multipoint correlations between spin and charge (density) in 2D Fermi-Hubbard systems and observed a simultaneous change across all presented observables around a specific doping δ_{FL} (Fig. 1A). We realized 2D Fermi-Hubbard systems at strong interactions $U/t = 7.4(8)$ or $U/t = 8.9(5)$ using ^{6}Li atoms in the lowest two hyperfine states in an optical lattice with spacing $a = 1.15\ \mu$m, as described in previous work (*28*). Full spin and density readout is achieved by detecting each spin component separately in adjacent layers of a vertical superlattice (*28*) (Fig. 1B). The Gaussian envelope of our optical beams creates a harmonic trapping potential, which naturally leads to an increasing hole doping from the center to the edge of our system. We use this spatial variation, together with our control of the total number of fermions in the system, to study the doping dependence of multipoint correlators (*33*). To explore all relevant hole-doping regimes, we use samples with up to ~100 atoms and temperatures down to $k_BT = 0.43(3)t$ (*33*), where k_B is the Boltzmann constant.

We study the connected part of bare N-point correlations, which contains the new information of order N (*34*), as illustrated in Fig. 1C. The disconnected part of bare correlations arises from lower-order contributions, whereas the connected part measures genuine higher-order effects.

The numerics we compare against are at finite temperature $k_BT = 0.4t$ and can be divided into three categories (Fig. 1D) [see (*33*) for details on all calculations]. We identify the FL regime at high doping, which we achieve by comparing to noninteracting (free) fermions and perturbation theory–related methods. In the low-doping regime, where FL concepts are expected to fail, we are interested in testing different approaches and their ability to capture low-doping physics. To this end, we include calculations for two versions of Anderson's resonating valence bond (RVB) states (*35*), namely uniform and π-flux, as well as a model for mutually independent magnetic polarons (string). Finally, we underscore key experimental observations of higher-order correlations with numerical calculations of the Fermi-Hubbard model. Therefore, we provide exact diagonalization (ED) of Fermi-Hubbard systems with 4×4 sites for which higher-order correlators can be readily implemented. Owing to finite size effects in the small cluster (*33*), we expect

[1]Max-Planck-Institut für Quantenoptik, 85748 Garching, Germany. [2]Munich Center for Quantum Science and Technology, 80799 München, Germany. [3]Department of Physics and Institute for Advanced Study, Technical University of Munich, 85748 Garching, Germany. [4]Department of Physics, Harvard University, Cambridge, MA 02138, USA. [5]Department of Physics and Astronomy, Clemson University, Clemson, SC 29631, USA. [6]Fakultät für Physik, Ludwig-Maximilians-Universität, 80799 München, Germany. [7]Institut für Laserphysik, Universität Hamburg, 22761 Hamburg, Germany. [8]The Hamburg Centre for Ultrafast Imaging, Universität Hamburg, 22761 Hamburg, Germany. [9]Physikalisches Institut, Eberhard Karls Universität Tübingen, 72076 Tübingen, Germany.
*Corresponding author. Email: joannis.koepsell@mpq.mpg.de
†Present address: Institute for Theoretical Atomic, Molecular and Optical Physics, Harvard-Smithsonian Center for Astrophysics, Cambridge, MA 02138, USA.
‡Present address: Department of Physics, Harvard University, Cambridge, MA 02138, USA.
§Present address: Institute for Theoretical Physics, ETH Zurich, 8093 Zurich, Switzerland.

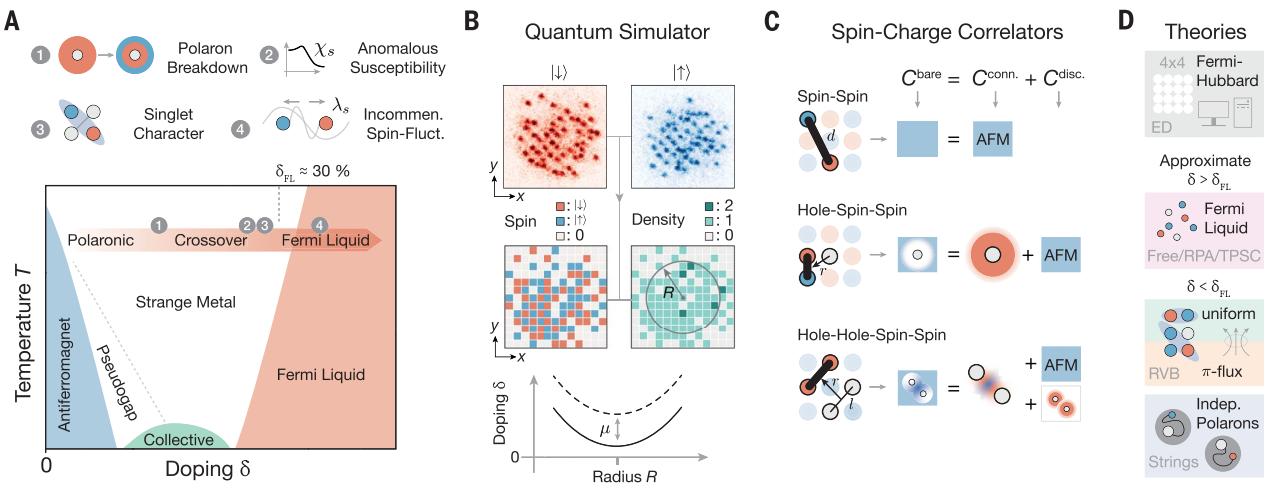

Fig. 1. Probing doped Mott insulators with spin-charge correlators. (**A**) Conjectured phase diagram of the 2D Fermi-Hubbard model upon hole doping δ and temperature T. Boundaries indicate crossovers between different regimes. Insets summarize our main experimental results. Incommen., incommensurate. (**B**) We independently image the two spin components of each Fermi-Hubbard realization with our quantum gas microscope. This enables reconstruction of the full spin and density (charge) information. The doping varies spatially in our harmonic trap and can be tuned by the total particle number to study the doping dependence of correlations. (**C**) Spin-spin, hole-spin-spin, and hole-hole-spin-spin correlators are analyzed in this work. As illustrated, bare multipoint correlations contain lower-order contributions and a connected part. For instance, in the magnetic polaron regime, a hole alters the antiferromagnetic environment in its vicinity. Therefore, bare hole-spin-spin correlations are reduced (white) close to the hole compared with the strong antiferromagnetic correlation at large distance (blue). The bare correlation (C^{bare}) can be decomposed into the genuine effect of the hole, that is, the connected part ($C^{conn.}$, red), and the antiferromagnetic (AFM) background value, that is, the disconnected part ($C^{disc.}$, blue). The sum of both parts corresponds to the bare correlation. Similarly, the genuine effect of a pair of holes on spin correlations (i.e., beyond single-hole effects) is quantified by the connected part of hole-hole-spin-spin correlations. This work focuses on connected correlations. (**D**) We compare experimental findings to exact diagonalization of 4×4 Fermi-Hubbard systems (top), mean-field–inspired approaches or free fermions approximating Fermi liquids at high doping (second from top), as well as three approaches (uniform-RVB, π-flux, and string), which are designed to capture the low-doping regime (bottom two panels). Indep., independent.

to find qualitative (rather than quantitative) agreements between ED and the experiment.

First, we investigate how the antiferromagnetic alignment of two spins at positions $\boldsymbol{r}_1$ and $\boldsymbol{r}_2$ evolves, by measuring connected two-point correlations (referred to as a bond)

$$C^{c}(\boldsymbol{d}) = C^{c}(\boldsymbol{r}_1, \boldsymbol{r}_2) = \eta\left(\langle \hat{S}^z_{\boldsymbol{r}_1} \hat{S}^z_{\boldsymbol{r}_2} \rangle - \langle \hat{S}^z_{\boldsymbol{r}_1} \rangle \langle \hat{S}^z_{\boldsymbol{r}_2} \rangle\right) \quad (1)$$

where we normalize by $\eta = 1/\left(\sigma\left(\hat{S}^z_{\boldsymbol{r}_1}\right)\sigma\left(\hat{S}^z_{\boldsymbol{r}_2}\right)\right)$, with σ denoting the standard deviation, and $\hat{S}^z_{\boldsymbol{r}}$ is the z component of the spin operator at position $\boldsymbol{r}$. The bond length, which is the distance between two spins, is given by $\boldsymbol{d} = \boldsymbol{r}_2 - \boldsymbol{r}_1$. If spin fluctuations are maximally correlated, the normalization η ensures that the correlator yields ±1. Therefore, quantitative values become comparable between different settings, because ±1 always means maximum possible positive or negative correlation. In the Heisenberg limit at half filling, η = 4, but for doped systems, η > 4.

As shown in Fig. 2A, doping quickly reduces the amplitude of antiferromagnetic correlations and leads to weakly oscillatory behavior as a function of doping. Between δ ~ 20 to 40%, spin correlations at different distances (such as $d = \sqrt{2}, 2, \sqrt{5}, \sqrt{8}$) reverse their sign as compared with their undoped value. We also find this phenomenon in our ED calculations (fig. S11). Therefore, many antiferromagnetic short-distance spin-spin correlations of the Mott insulator undergo a fundamental change in a crossover region at doping of δ = 20 to 40%. From this doping regime onward, spin-spin correlations of a FL (free) start to agree with experimental data (fig. S11).

The uniform-RVB state features sign flips of correlations similar to experimental data and also compares well for larger dopings. The string model and π-flux behave similarly and show agreement with our data for δ < 20%, in line with (*24*). Predictions for two-point correlations of different theoretical approaches are very similar at low doping, which calls for a comparison of higher-order spin-charge correlations.

In the FL, above hole concentrations around 50%, oscillating magnetism manifests itself as visible peaks in the static spin-structure factor $S(\boldsymbol{q})$ shifting from (π, π) toward (π, 0). The effect is even more pronounced in an adjusted version $S^*(\boldsymbol{q})$ (Fig. 2, B and C), which neglects the strong on-site term $d = 0$ equivalent to a broad offset in Fourier space (*33*). This shift of fluctuations toward momenta incommensurate with the lattice spacing is in excellent agreement with a perturbation theory–inspired two-particle-self-consistent approach (TPSC) (*36*) and confirms quantum Monte Carlo (QMC) calculations (*37*, *38*). The observed shift of spin fluctuations can be considered a FL phenomenon, where a stretch of the Fermi wave vector $\boldsymbol{q}_F$ with increasing doping causes such incommensurate fluctuations through interactions on a mean-field level. Establishing a connection to incommensurate spin-density wave phases (stripes) at weak doping and colder temperatures (*39*) requires further exploration.

Furthermore, we extract the doping dependence of the uniform ($\boldsymbol{q} = 0$) spin susceptibility χ_s (Fig. 2D) by applying the fluctuation-dissipation relation (*33*) in an approach similar to that described in (*25*, *40*). To identify behavior not captured by (i.e., anomalous to) mean-field–related methods, we compare experimental data with three FL-type calculations: free fermions without interaction, a random phase approximation (RPA), and TPSC. The interaction U can be considered a free effective parameter for RPA calculations, and we chose $U/t = 4$ to avoid divergences (*33*). Down to $\delta = \delta_{FL} \sim 30\%$, the susceptibility increases with decreasing doping, which is quantitatively best captured by TPSC calculations. However, below δ_{FL}, the susceptibility χ_s stops increasing for weaker dopings. This bendover behavior is reminiscent of the pseudogap phenomenon as well as

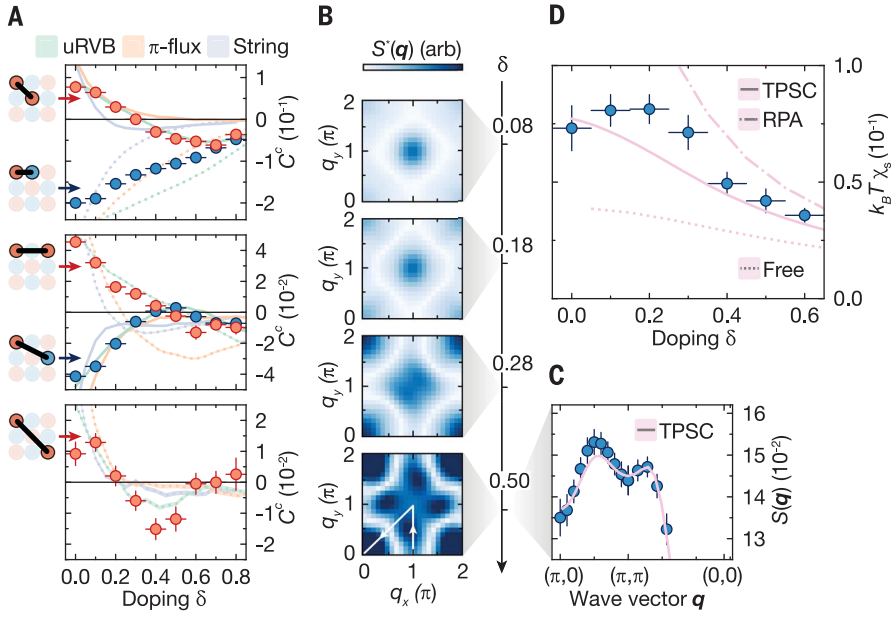

Fig. 2. Magnetism from Mott insulator to Fermi liquid. (**A**) Connected two-point spin correlations as a function of doping for different spin distances. Red (blue) experimental data points correspond to spin distances with positive (negative) correlation at half filling (see arrows to insets). Error bars denote one standard error of the mean (SEM) and for doping the bin width for averaging. Solid (dotted) lines of numerical calculations indicated in the legend correspond to spin distances of red (blue) data points. Shaded bands indicate the statistical SEM for all calculations where visible. (**B**) Measured static spin-structure factor $S^*(\boldsymbol{q})$ [without on-site term, see (*33*)] for increasing doping with arbitrary (arb) scales. (**C**) Trace through spin-structure factor $S(\boldsymbol{q})$ at 50% doping. Error bars are representative also for lower dopings. The full width of doping bins for (B) and (C) is 0.14. Solid pink represents a mean-field–related TPSC calculation. (**D**) Doping dependence of the uniform magnetic susceptibility, obtained via the fluctuation-dissipation relation from experimental data. Solid, dot-dashed, and dotted pink curves correspond to TPSC, RPA, and free fermion calculations, respectively. This figure is based on 3224 experimental realizations at $k_B T = 0.43(3)t$ and $U/t = 8.9(5)$.

anomalous with respect to (i.e., not captured by) our FL calculations. QMC results (*41*) support this observation, which indicates that the metallic regime close to the Mott insulator and below δ_{FL} is of a different nature than the conventional FL found at higher dopings [for convergence of structure factors in FL, see (*33*)].

The weakly doped metallic regime hosts magnetic polarons, whose dressing cloud can be measured with a three-point correlator of two spins around a hole (*16*, *29*). We now investigate how this dressing cloud evolves when the system turns into a conventional FL at strong doping.

We consider the connected part of hole-spin-spin correlations (*33*), which for spin-balanced systems $\langle \hat{S}^z_{\boldsymbol{r}_i} \rangle = 0$ simplifies to

$$C^c_\circ(\boldsymbol{r}, \boldsymbol{d}) = C^c_\circ(\boldsymbol{r}_3; \boldsymbol{r}_1, \boldsymbol{r}_2) = \eta \left\langle \hat{S}^z_{\boldsymbol{r}_1} \hat{S}^z_{\boldsymbol{r}_2} \right\rangle_{\circ_{\boldsymbol{r}_3}} - C^c(\boldsymbol{r}_1, \boldsymbol{r}_2) \quad (2)$$

This correlator measures how a spin-spin bond is perturbed away from the background two-point correlation by a (post-selected) hole, denoted by the empty-circle symbol, at a third position $\boldsymbol{r}_3$ (compare Fig. 1C). The distance of the bond center to the hole is given by $\boldsymbol{r} = (\boldsymbol{r}_1 + \boldsymbol{r}_2)/2 - \boldsymbol{r}_3$.

For δ around 10%, a hole perturbs all bonds in its vicinity with a sign opposite to the antiferromagnetic background. This means that NN spins ($d = 1$) align more parallel (positive connected correlation) and diagonal spins ($d = \sqrt{2}$) more antiparallel (negative connected correlation) (Fig. 3). Such connected correlations oppose the background antiferromagnetic spin-spin correlations and are characteristic of magnetic polarons (polaronic correlations), that is, a direct manifestation of their dressing cloud. Doublon-hole fluctuations cause a similar connected signal at half filling but play a minor role at 10% doping (*33*). Connected correlations fall off with increasing bond distance from the hole. We measure the radial dependence of the polaronic dressing by plotting NN and diagonal correlations as a function of bond distance from the hole (Fig. 3C). Because this illustration combines two different bond lengths d, we reverse the sign of diagonal correlations [multiplication by $(-1)^{d^2+1}$], such that a positive value indicates a connected correlation opposing the antiferromagnetic correlations of the Mott insulator.

In the FL regime at large doping, we observe a negative connected correlation of all bonds (also $d = 1$) in the presence of a hole. The connected correlation has the same sign as the negative NN and diagonal spin-spin correlations at strong doping (compare Fig. 2A). Hence, the presence of the hole enhances (i.e., does not oppose) spin correlations. We interpret negative connected hole-spin-spin correlations in the FL regime to be caused by the Pauli exclusion principle, which leads to anticorrelation of fermions in an area increasing with doping (*25*). The post-selected hole restricts spins to a smaller area and increases the observed anticorrelation.

Therefore, holes oppose magnetic two-point correlations at weak doping (magnetic polarons) but enhance them at strong doping (FL). A useful indicator to study the transition between these two metallic regimes is the NN bond ($d = 1$) closest to the hole. Its connected correlation continuously evolves from positive to negative across the regimes (while two-point NN correlations remain negative for all dopings) (Fig. 3D). An initial drop of the connected signal is expected from the higher concentration of polarons, as their dressing clouds start to overlap. Around 20% doping, the closest NN bond becomes uncorrelated with the presence of the hole and builds up a negative correlation toward δ_{FL}, consistent with ED. Connected correlations of closest-distance diagonal bonds are negative for all dopings with a slight minimum around doping $\delta \sim \delta_{FL}$. This dip can most likely be explained by the effect of holes created during the detection process on measured correlations close to half filling. We performed an analysis of systematic effects from detection infidelities to exclude effects on other reported findings (*33*). In Fig. 3D, we provide an estimate for the renormalization of correlations caused by detection holes (*33*), represented by points with dashed edges.

String and RVB predictions for $C^c_\circ$ are very distinguishable at weak dopings. Only the polaron model (string) reproduces the experimental ferromagnetic alignment of the closest NN bond, whereas RVB states show strong discrepancies to experiment. Uniform RVB is a prime example of how a theoretical approach can show excellent agreement with experiment in two-point correlations at low doping but reveal strong deviations at higher-order correlators. At large dopings, uniform RVB and free fermions start to capture the correlations driven by fermionic statistics.

QMC studies of Fermi-Hubbard systems found the bandwidth of quasiparticle excitations

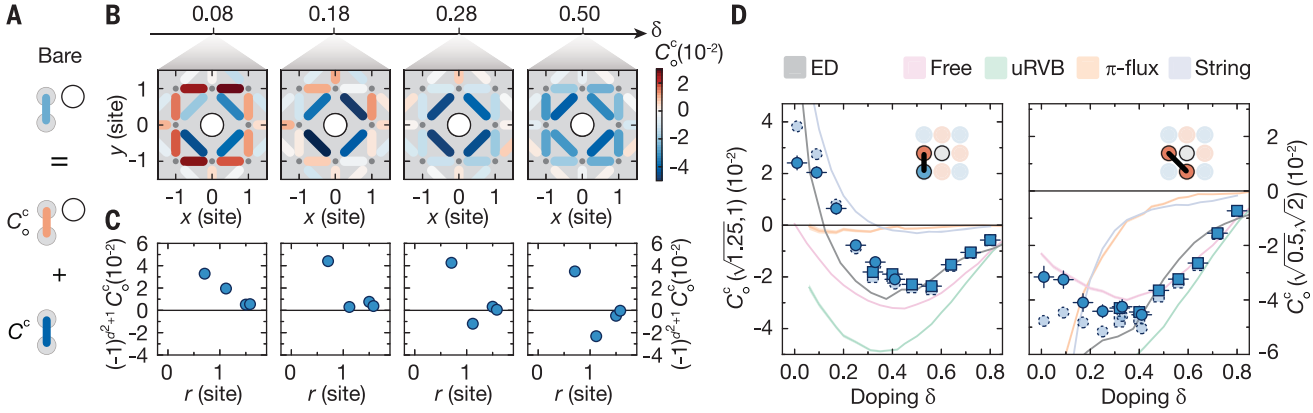

Fig. 3. Breakdown of polaronic correlations. (**A**) Relation between bare and connected spin correlations in the vicinity of a hole. (**B**) Connected correlation (represented as bonds) of spins on NN and diagonal lattice sites (gray dots) in the presence of a single hole (white central dot) for different dopings. The SEM for individual bonds is on the order of 0.5×10^{-2}. (**C**) Averaging connected correlations of (B) ($d = 1$ and $d = \sqrt{2}$) as a function of bond distance r from the hole, where we flip the sign of correlations with bond length $d = \sqrt{2}$. Thus, a positive correlation indicates a connected signal opposing the two-point correlations at half filling. Error bars denote one SEM and are smaller than the point size. The full width of doping bins for (B) and (C) is 0.1. (**D**) Doping dependence of the NN and diagonal bonds closest to the hole (see insets). Square (circular) data points were extracted from a dataset with an average of 52.0(1) [91.3(1)] particles. Points with dashed edges take into account estimates for the effect of detection infidelities of this dataset (*33*). Solid lines represent numerical calculations (see legend), and shaded bands indicate (where visible) their statistical SEM. This figure is based on 18,107 experimental realizations at $k_B T = 0.52(5)t$ and $U/t = 7.4(8)$.

evolves from polaronic (order $2J$) to Fermi liquid (order $8t$) at around 30% doping (*42*). Our measurements suggest that polaronic dressing persists up to $\delta \sim 20\%$ and smoothly dissolves into correlations of a FL (free) around $\delta_{FL} \sim 30\%$.

When two polarons come close, their dressing clouds overlap, which can either lead to the breakdown of polarons or induce effective interactions between them. This is often considered a possible mechanism for pseudogap behavior (*1*, *2*, *43*). Hole-hole correlators do not show indications of hole binding at current temperatures of cold-atom quantum simulators (*24*, *29*, *33*), hence we search for interaction signatures in the magnetic environment of two holes.

In the analysis, we post-select on two holes at positions $\boldsymbol{r}_3$ and $\boldsymbol{r}_4$ and evaluate the connected (four-point) correlation between two spins in the presence of a hole pair, which in a spin-balanced system reduces to

$$C^c_{\circ\circ}(\boldsymbol{l},\boldsymbol{r},\boldsymbol{d}) = C^c_{\circ\circ}(\boldsymbol{r}_3,\boldsymbol{r}_4;\boldsymbol{r}_1,\boldsymbol{r}_2) = \eta\left\langle \hat{S}^z_{\boldsymbol{r}_1}\hat{S}^z_{\boldsymbol{r}_2}\right\rangle_{\circ_{\boldsymbol{r}_3}\circ_{\boldsymbol{r}_4}} - C^c(\boldsymbol{r}_1,\boldsymbol{r}_2) - \gamma\left(C^c_{\circ}(\boldsymbol{r}_3;\boldsymbol{r}_1,\boldsymbol{r}_2) + C^c_{\circ}(\boldsymbol{r}_4;\boldsymbol{r}_1,\boldsymbol{r}_2)\right) \quad (3)$$

The composition of this correlator is illustrated in Fig. 4A, and for the general expression, see (*33*). The mutual distance of the holes is defined as $\boldsymbol{l} = \boldsymbol{r}_4 - \boldsymbol{r}_3$, and the bond distance $\boldsymbol{r}$ is measured with respect to the center of $\boldsymbol{l}$. $C^c_{\circ\circ}$ detects correlations linked to the presence of the holes as a pair and measures how much these deviate from a simple addition of two independent single-hole signals $C^c_{\circ}$ with a weighting factor $\gamma = \left\langle \hat{h}_{\boldsymbol{r}_3}\right\rangle\left\langle \hat{h}_{\boldsymbol{r}_4}\right\rangle / \left\langle \hat{h}_{\boldsymbol{r}_3}\hat{h}_{\boldsymbol{r}_4}\right\rangle$ and hole density operator $\hat{h}_{\boldsymbol{r}_i}$.

We study the case of NN ($l = 1$) or diagonal ($l = \sqrt{2}$) hole pairs and bonds $d = 1, \sqrt{2}$. To obtain a sufficient signal-to-noise ratio in the experiment, we combine the two configurations for NN [$\boldsymbol{l} = (1,0),(0,1)$] and diagonal pairs [$\boldsymbol{l} = (1,1),(1,-1)$] by averaging all bonds with identical bond distance r from the pair. To visualize correlations, we choose a representation in terms of $\boldsymbol{l} = (1,0)$ and $\boldsymbol{l} = (1,1)$ (Fig. 4B). We find connected antiferromagnetic alignment of bonds at closest distance to the pair, which connects both metallic regimes. As shown in Fig. 4, B and C, for NN holes, the closest bond has a negative correlation at half filling [inherited from doublon-hole pairs (*33*)], which stays antiferromagnetic for higher doping and quantitatively agrees with correlations of a FL (free) for $\delta > \delta_{FL}$. This bond is furthermore robust against an increase in temperature to $k_B T = 0.77(7)t$. For diagonal holes, the diagonal spin bond between them has the shortest distance to the pair (Fig. 4, B and C). This bond is uncorrelated at half filling [doublon-hole pairs contribute a ferromagnetic signal; see ED at $\delta = 0\%$ or (*33*)], then rapidly turns antiferromagnetic with doping, peaks at $\delta_{FL} \sim 30\%$, and is eventually described quantitatively by correlations of a Fermi liquid (free) for $\delta > \delta_{FL}$. For higher temperatures, the correlation of this bond is substantially reduced. A possible systematic effect of detection holes on correlations [see (*33*)] does not alter our findings and is indicated in Fig. 4C as points with dashed edges. Approximate theories for low doping partly predict such antiferromagnetic correlations of closest distance bonds but show limited overall agreement to experimental data.

To gain insight into how such correlations would connect to lower-temperature physics, we consider two holes ($\delta \sim 2\%$) in the t-J model, for which binding of polarons (holes) occurs at relatively high temperatures (*44*). We performed density matrix renormalization group (DMRG) calculations of this scenario at $T = 0$ for a six-leg ladder (*33*) and show the connected spin environment in Fig. 4D for $l = 1$ and $l = \sqrt{2}$. A notable effect of hole pairing is the emergence of a strong antiferromagnetic spin bond at closest distance to the pair, suggesting local singlet formation (*44*, *45*). Our experimental data feature qualitatively similar negative correlations (reminiscent of this singlet character) but no further indication of hole binding [see hole-hole correlations in (*33*)]. Hence, correlations already existing at our experimental temperatures could smoothly connect to correlations of possible hole pairing scenarios at colder temperatures.

In this study, we measured how correlations in antiferromagnetic Mott insulators evolve with increasing doping, and we revealed a metal of magnetic polarons at weak doping and a Fermi liquid at dopings larger than $\delta_{FL} \sim 30\%$. The distinctive capability of our quantum simulator enabled us to study the continuous doping dependence of observables unavailable in traditional solid-state experiments. A transition between the two metallic regimes is signaled

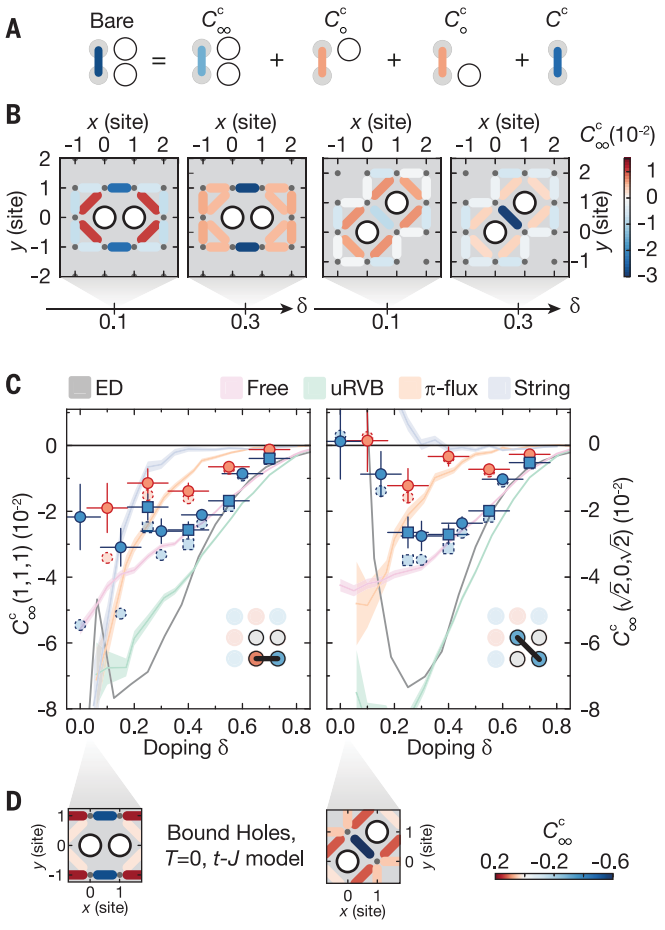

Fig. 4. Influence of two holes on spin correlations. (**A**) Relation between bare and connected spin correlations in the vicinity of two holes. (**B**) Connected correlations of NN and diagonal spins in the presence of a NN or diagonal pair of holes at an experimental temperature of 0.52(5)*t*. Two dopings with a full width of the doping bin of 0.2 are shown for NN and diagonal holes. Same bond distances and symmetric spatial hole orientations are averaged together (see text). (**C**) Connected correlation of the bond with closest distance to the NN or diagonal hole pair (see insets) as a function of doping. Blue (red) points correspond to experimental temperatures of 0.52(5)*t* [0.77(7)*t*]. Blue square (circular) data points were extracted from a dataset with an average of 52.0(1) [91.3(1)] particles. Points with dashed edges take into account estimates for the effect of detection infidelities of this dataset (*33*). Solid lines represent numerical calculations, as indicated (see legend), and shaded bands, their statistical SEM. (**D**) DMRG calculations (T = 0) for two holes in the six-leg ladder t-J model, where binding occurs. (B) and (C) of this figure are based on 23,695 experimental realizations at U/t = 7.4(8).

across all studied system properties (for a summary, see table S1), and the intricate spin-charge correlations reported serve as a basis to develop a microscopic understanding of pseudogap or collective phenomena at colder temperatures. How the observed doping for this crossover in our experiment can be related to solid-state measurements is unclear because details such as band structure and the difference in accessed observables play an important role. In a benchmark of three approximate low-doping theories, we find limited overall agreement with our system, which calls for more effective descriptions. Spin-charge correlators could also be studied in out-of-equilibrium systems (*23*, *30*,), and even modest progress in achieving colder temperatures with available cooling proposals (*46*) might enable experimental observation of pairing (*44*) and pseudogap behavior (*47*). Future studies could focus on fifth-order (*48*) correlators to further solidify our understanding of exotic many-body phenomena and test different theories (*49*, *50*).

REFERENCES AND NOTES

1. B. Keimer, S. A. Kivelson, M. R. Norman, S. Uchida, J. Zaanen, *Nature* **518**, 179–186 (2015).
2. E. Dagotto, *Rev. Mod. Phys.* **66**, 763–840 (1994).
3. P. A. Lee, N. Nagaosa, X.-G. Wen, *Rev. Mod. Phys.* **78**, 17–85 (2006).
4. S. Badoux *et al.*, *Nature* **531**, 210–214 (2016).
5. S. D. Chen *et al.*, *Science* **366**, 1099–1102 (2019).
6. N. Doiron-Leyraud *et al.*, *Nature* **447**, 565–568 (2007).
7. H.-B. Yang *et al.*, *Phys. Rev. Lett.* **107**, 047003 (2011).
8. F. Ronning *et al.*, *Phys. Rev. B* **71**, 094518 (2005).
9. J. R. Schrieffer, *Handbook of High-Temperature Superconductivity* (Springer, 2007).
10. L. Bulaevski, É. Nagaev, D. Khomskiĭ, *Sov. J. Exp. Theor. Phys.* **27**, 836 (1968).
11. S. Schmitt-Rink, C. M. Varma, A. E. Ruckenstein, *Phys. Rev. Lett.* **60**, 2793–2796 (1988).
12. B. I. Shraiman, E. D. Siggia, *Phys. Rev. Lett.* **61**, 467–470 (1988).
13. C. L. Kane, P. A. Lee, N. Read, *Phys. Rev. B* **39**, 6880–6897 (1989).
14. S. Sachdev, *Phys. Rev. B* **39**, 12232–12247 (1989).
15. F. Grusdt *et al.*, *Phys. Rev. X* **8**, 011046 (2018).
16. E. Blomquist, J. Carlström, *Commun. Phys.* **3**, 172 (2020).
17. M. Frachet *et al.*, *Nat. Phys.* **16**, 1064–1068 (2020).
18. P. F. LeBlanc *et al.*, *Phys. Rev. X* **5**, 041041 (2015).
19. B.-B. Chen *et al.*, *Phys. Rev. B* **103**, L041107 (2021).
20. C. Gross, I. Bloch, *Science* **357**, 995–1001 (2017).
21. M. A. Nichols *et al.*, *Science* **363**, 383–387 (2019).
22. P. T. Brown *et al.*, *Science* **363**, 379–382 (2019).
23. G. Ji *et al.*, *Phys. Rev. X* **11**, 021022 (2021).
24. C. S. Chiu *et al.*, *Science* **365**, 251–256 (2019).
25. T. Hartke, B. Oreg, N. Jia, M. Zwierlein, *Phys. Rev. Lett.* **125**, 113601 (2020).
26. A. Mazurenko *et al.*, *Nature* **545**, 462–466 (2017).
27. M. Boll *et al.*, *Science* **353**, 1257–1260 (2016).
28. J. Koepsell *et al.*, *Phys. Rev. Lett.* **125**, 010403 (2020).
29. J. Koepsell *et al.*, *Nature* **572**, 358–362 (2019).
30. J. Vijayan *et al.*, *Science* **367**, 186–189 (2020).
31. G. Salomon *et al.*, *Nature* **565**, 56–60 (2019).
32. T. A. Hilker *et al.*, *Science* **357**, 484–487 (2017).
33. See supplementary materials.
34. T. Schweigler *et al.*, *Nature* **545**, 323–326 (2017).
35. P. W. Anderson, *Science* **235**, 1196–1198 (1987).
36. Y. M. Vilk, L. Chen, A. Tremblay, *Phys. Rev. B* **49**, 13267–13270 (1994).
37. A. Moreo, D. J. Scalapino, R. L. Sugar, S. R. White, N. E. Bickers, *Phys. Rev. B* **41**, 2313–2320 (1990).
38. N. Furukawa, M. Imada, *J. Phys. Soc. Jpn.* **61**, 3331–3354 (1992).
39. S. W. Cheong *et al.*, *Phys. Rev. Lett.* **67**, 1791–1794 (1991).
40. J. H. Drewes *et al.*, *Phys. Rev. Lett.* **117**, 135301 (2016).
41. A. Moreo, *Phys. Rev. B* **48**, 3380–3382 (1993).
42. R. Preuss, W. Hanke, C. Gröber, H. G. Evertz, *Phys. Rev. Lett.* **79**, 1122–1125 (1997).
43. J. R. Schrieffer, X. G. Wen, S. C. Zhang, *Phys. Rev. B* **39**, 11663–11679 (1989)
44. E. Blomquist, J. Carlström, *Phys. Rev. Res.* **3**, 013272 (2021).
45. S. R. White, D. Scalapino, *Phys. Rev. B* **55**, R14701–R14704 (1997).
46. A. Kantian, S. Langer, A. J. Daley, *Phys. Rev. Lett.* **120**, 060401 (2018).
47. E. Khatami, M. Rigol, *Phys. Rev. A* **84**, 053611 (2011).
48. A. Bohrdt *et al.*, *Phys. Rev. Lett.* **126**, 026401 (2021).
49. M. Punk, A. Allais, S. Sachdev, *Proc. Natl. Acad. Sci. U.S.A.* **112**, 9552–9557 (2015).
50. Y.-H. Zhang, S. Sachdev, *Phys. Rev. Res.* **2**, 023172 (2020).
51. J. Koepsell, Data and code for Microscopic evolution of doped Mott insulators from polaronic metal to Fermi liquid, Max Planck Society (2021); https://dx.doi.org/10.17617/3.6l.

ACKNOWLEDGMENTS

The authors thank T. A. Hilker and T. Chalopin for insightful discussions and careful reading of the manuscript. **Funding:** This work was supported by the Max Planck Society (MPG), the European Union (FET-Flag 817482, PASQUANS), the Max Planck Harvard Research Center for Quantum Optics (MPHQ), and Germany's Excellence Strategy – EXC-2111 – 390814868. This research used resources of the National Energy Research Scientific Computing Center (NERSC), a US Department of Energy Office of Science User Facility operated under contract DE-AC02-05CH11231. J.K. gratefully acknowledges funding from the Hector Fellow Academy. E.D. and Y.W. acknowledge support from Harvard-MIT CUA, ARO grant W911NF-20-1-0163, and the National Science Foundation through grant OAC-1934714. Y.W. acknowledges support from the National Science Foundation award DMR-2038011. **Author contributions:** All authors contributed substantially to the work presented in this manuscript. J.K., D.B., P.S., and S.H. acquired the data and maintained the experimental apparatus. J.K. and G.S. analyzed the data. J.K. prepared the manuscript. A.B., Y.W., F.G., and E.D. performed the numerical calculations. C.G. and I.B. supervised the study. All authors worked on the interpretation of the data and contributed to the final manuscript. **Competing interests:** The authors declare no competing interests. **Data and materials availability:** Data displayed in the plots and code associated with numerical calculations of this paper are publicly available from the Open Access Data Repository of the Max Planck Society (*51*).

SUPPLEMENTARY MATERIALS

science.org/doi/10.1126/science.abe7165
Supplementary Text
Figs. S1 to S12
Table S1
References (*52*–*61*)

9 September 2020; accepted 21 August 2021
10.1126/science.abe7165

Science

Microscopic evolution of doped Mott insulators from polaronic metal to Fermi liquid

Joannis KoepsellDominik BourgundPimonpan SompetSarah HirtheAnnabelle BohrdtYao WangFabian GrusdtEugene DemlerGuillaume SalomonChristian GrossImmanuel Bloch

Science, 374 (6563), • DOI: 10.1126/science.abe7165

From polarons to a Fermi liquid

Superconductivity in the cuprates emerges by doping an antiferromagnetic "parent" state with holes or electrons. With increased doping, antiferromagnetism gives way to unconventional superconductivity, and the system eventually becomes a Fermi liquid. Koepsell *et al*. simulated this progression using cold, strongly interacting lithium-6 atoms trapped in an optical lattice. Although the equivalent ordered phases are not yet reachable at the experimentally available temperatures, the researchers were able to measure multipoint spin and hole correlations over a wide range of hole doping. The evolution of these correlators with doping revealed a crossover from a polaronic regime to a Fermi liquid. —JS